This is the peer reviewed version of the following article: Martinez-Agirre, A., Álvarez-Mozos, J., Milenković, M., Pfeifer, N., Giménez, R., Valle, J. M., and Rodríguez, Á. (2020) Evaluation of Terrestrial Laser Scanner and Structure from Motion photogrammetry techniques for quantifying soil surface roughness parameters over agricultural soils. Earth Surf. Process. Landforms, 45: 605– 621, which has been published in final form at https://doi.org/10.1002/esp.4758. This article may be used for non-commercial purposes in accordance with Wiley Terms and Conditions for Use of Self-Archived Versions.

Evaluation of Terrestrial Laser Scanner and Structure from Motion photogrammetry techniques for quantifying soil surface roughness parameters over agricultural soils

Alex Martinez-Agirre[1*], Jesús Álvarez-Mozos[1], Milutin Milenković[2,3], Norbert Pfeifer[4], Rafael Giménez[1], José Manuel Valle Melón[5] and Álvaro Rodríguez Miranda[5]

[1] Department of Engineering, Public University of Navarre, Pamplona, Spain

[2] Laboratory of Geo-information Science and Remote Sensing, Department of Environmental Science, Wageningen University, Wageningen, The Netherlands

[3] Geological Survey of Austria, Vienna, Austria

[4] Department of Geodesy and Geoinformation (GEO), Technische Universität Wien, Vienna, Austria

[5] Laboratory for the Geometric Documentation of Heritage (GPAC – Built Heritage Research Group), University of the Basque Country, Vitoria-Gasteiz, Spain.

*Corresponding Author: Phone: (34) 948168937. E-mail: alejandro.mda@unavarra.es

Highlights

- Terrestrial Laser Scanner (TLS) and Structure from Motion (SfM) photogrammetry techniques were evaluated for quantifying surface roughness over different agricultural soils.
- A precise co-registration of TLS and SfM photogrammetry point-clouds with laser profilometer data was carried out to compare different roughness parameters.
- Profiles obtained with SfM photogrammetry and TLS (to a lesser extent) showed lower high-frequency elevation information that affected the values of some roughness parameters when compared to the laser profilometer.
- TLS and SfM photogrammetry proved to be useful for measuring 3D soil surface roughness in agricultural soils.

Abstract

The surface roughness of agricultural soils is mainly related to the type of tillage performed, typically consisting of oriented and random components. Traditionally, soil surface roughness (SSR) characterization has been difficult due to its high spatial variability and the sensitivity of roughness parameters to the characteristics of the instruments, including its measurement scale. Recent advances in surveying have greatly improved the spatial resolution, extent, and availability of surface elevation datasets. However, it is still unknown how new

roughness measurements relates with the conventional roughness measurements such as 2D profiles acquired by laser profilometers. The objective of this study was to evaluate the suitability of Terrestrial Laser Scanner (TLS) and Structure from Motion (SfM) photogrammetry techniques for quantifying SSR over different agricultural soils. With this aim, an experiment was carried out in three plots (5 × 5 m) representing different roughness conditions, where TLS and SfM photogrammetry measurements were co-registered with 2D profiles obtained using a laser profilometer. Differences between new and conventional roughness measurement techniques were evaluated visually and quantitatively using regression analysis and comparing the values of six different roughness parameters. TLS and SfM photogrammetry measurements were further compared by evaluating multi-directional roughness parameters and analyzing corresponding Digital Elevation Models. The results obtained demonstrate the ability of both TLS and SfM photogrammetry techniques to measure 3D SSR over agricultural soils. However, profiles obtained with both techniques (especially SfM photogrammetry) showed a loss of high-frequency elevation information that affected the values of some parameters (e.g. initial slope of the autocorrelation function, peak frequency and tortuosity). Nevertheless, both TLS and SfM photogrammetry provide a massive amount of 3D information that enables a detailed analysis of surface roughness, which is relevant for multiple applications, such as those focused in hydrological and soil erosion processes and microwave scattering.

Keywords: soil surface roughness, TLS, SfM photogrammetry, roughness parameters, agricultural soils

Introduction

Soil Surface Roughness (SSR, also referred to as micro-topography or micro-relief) can be defined differently depending primarily on its application. For example, in the radar scattering theory, SSR is defined as the variation in soil surface elevation relative to a reference surface (Ulaby et al., 1982). In agricultural soils, SSR is mainly an anthropogenic factor determined by the type of tillage and management, typically with an oriented component consisting of pseudo-periodical height variations due to tillage implements and a random component representing soil clods or aggregates. In agricultural soils, SSR is a property with a high spatial variability, since the same type of tillage can result in surfaces with different SSRs depending on the physical characteristics of the soil. In addition, SSR is more or less susceptible to change through time due to the action of meteorological agents (e.g., precipitation, wind and temperature changes) in the low atmosphere or even animal activity (Martinez-Agirre et al., 2016).

SSR is a key element in hydrology and soil erosion processes occurring at the soil-atmosphere interface (Helming et al., 1998), such as infiltration, runoff, the detachment of soil particles due to water or wind, gas exchange, evaporation, and heat fluxes (Huang and Bradford, 1992). Therefore, quantifying SSR can be useful for understanding and modeling processes relevant for different applications.

Many different parameters and indices have been proposed for quantifying SSR (e.g., Helming et al., 1993; Magunda et al., 1997; Kamphorst et al., 2000; Taconet and Ciarletti, 2007; Vermang et al., 2013). These can be divided into four groups (Martinez-Agirre et al., 2016), following a criterion similar to that of Smith (2014): (1) parameters measuring the vertical dimension of roughness, (2) parameters measuring the horizontal dimension of roughness, (3) parameters combining both dimensions, and (4) parameters based on fractal theory. The first parameters measure the magnitude of elevation differences along a transect or area. On the other hand, horizontal parameters evaluate the spacing at which these elevation differences occur. Combined parameters represent both properties since they are normally obtained as the product or ratio of a vertical and a horizontal parameter. Finally, fractal parameters measure the self-affinity of surface transects or areas, i.e., whether similar statistical properties can be obtained at different spatial scales along the surface. Although the number of parameters found in the literature is high, many of them measure similar properties and are, thus, strongly correlated (Martinez-Agirre et al., 2016). Depending on the particular application of interest, some parameters have been preferred to others, with the standard deviation of heights (s) (also referred to as RMS of height) being the most commonly used in most applications (Govers et al., 2000; Verhoest et al., 2008). Recent advances in surveying have greatly improved the spatial resolution, extent, and availability of surface elevation datasets (Smith, 2014). Surface roughness measurement techniques can be classified according to various criteria: the dimensionality of measure (2D/3D), resolution (mm/cm), sensor type, and whether the measure is done with contact to the soil surface or not (Jester and Klik, 2005; Gilliot et al., 2017). However, most of the literature in the topic

centered the classification into contact and non-contact techniques (Govers et al., 2000; Verhoest et al., 2008, Aguilar et al., 2009; Thomsen et al., 2015; Nouwakpo et al., 2016). Regarding this, non-contact devices are preferred because the physical contact between an instrument and the soil surface is associated with measurement biases and disturbances (Jester and Klik, 2005). For example, a laser profilometer is a non-contact instrument that records surface elevations along a transect (i.e., a 2D surface profile) with a given length and a regular sampling interval. For many years, this technique has been the standard for SSR measurements in different fields of earth science (e.g., microwave remote sensing, soil erosion) (Helming et al., 1998; Davidson et al., 2000; Jester and Klik, 2005). However, 3D laser scanning and image-based 3D reconstruction techniques have been recently suggested as alternatives for the traditional non-contact SSR measurements (Barneveld et al., 2013, Nouwakpo et al., 2016).

Image-based 3D reconstruction techniques are nowadays primarily based on Structure from Motion (SfM) principles. SfM photogrammetry combines the utility of digital photogrammetry with a flexibility and ease of use derived from multi-view computer vision methods (James et al., 2019). In contrast to traditional and close-range oblique photogrammetry, SfM photogrammetry relaxes some constraints (i.e., calibration, collinearity equations and orientation) making image acquisition and processing significantly easier for non-expert users (Castillo et al., 2012; James and Robson, 2012; Woodget et al., 2015; Gomez et al., 2015; Nouwakpo et al., 2016; Mosbrucker et al., 2017; James et al., 2019). Therefore, the interest of scientists in this technology has expanded across different disciplines in geosciences, due also to the development of readily available SfM photogrammetry software (Nouwakpo et al., 2016).

Laser-based technologies, also known as laser scanning or LiDAR (light detection and ranging), have also been used for high-resolution soil micro-topography measurements (Perez-Gutierrez et al., 2007; Aguilar et al., 2009; Castillo et al., 2012; Milenković et al., 2015; Nouwakpo et al., 2016). Specifically, Terrestrial Laser Scanner (TLS) can reach accuracies down to 0.1 mm. Although TLS's high hardware acquisition cost and bulky size have limited its widespread use for field measurement campaigns (Nouwakpo et al., 2016), technical improvements in sensor design might improve this in the near future.

Table 1. Studies published using TLS and/or photogrammetry techniques (SfM or not) for measuring surface roughness in agricultural soils.

Reference	Techniques	Roughness classes	Size of plots
Gilliot et al., 2017	SP	4 (from moldboard to rotary cultivator)	0.54 × 0.44 m
Nouwakpo et al., 2016	TLS/SfM	No tilled (bare ground)	6 × 2 m
Rodriguez-Caballero et al., 2016	TLS	2 (barley field and natural hillslope)	-
Milenković et al., 2015	TLS/OTS	Seedbed	2.6 × 3 m
Thomsen et al., 2015	TLS/SP/Others	4 (harrowed, ploughed, seeding and forest)	1 × 1 m
Snapir et al., 2014	SfM	No tilled	2 × 11 m
Barneveld et al., 2013	TLS	3 (moldboard, harrowed and seedbed)	21 – 100 m^2
Marzahn et al., 2012a	SP	6 (from moldboard to seedbed)	1 × 2.5 m
Mirzaei et al., 2012	SP	2 (harrowed and seedbed)	1 × 1 m
Heng et al., 2010	TLS/SP	No tilled	3.9 × 1.4 m
Aguilar et al., 2009	TLS/SP	2 (untilled and very cloddy tilled)	0.2 m^2
Blaes and Defourny, 2008	PRO/SP	3 (sugar beet, winter wheat and maize)	8 m^2
Taconet and Ciarletti, 2007	SP	3 (from chisel to seedbed)	0.5 – 3.5 m^2
Jester and Klik, 2005	TLS/SP	2 (smooth and rough)	0.55 × 0.5 m

OTS = Optical Triangulating Scanner; SP = Stereo-photogrammetry; PRO = Laser profilometer

Different studies have already attempted to measure SSR with TLS and photogrammetry techniques (SfM or not) (Table 1). Many of these considered either one measurement technique, or just one single soil roughness condition (Taconet and Ciarletti, 2007; Heng et al., 2010; Mirzaei et al., 2012; Snapir et al., 2014; Milenković et al., 2015; Rodriguez-Caballero et al., 2016; Nouwakpo et al., 2016). Other studies focused more on a comparison between old and new techniques (Jester and Klik, 2005; Thomsen et al., 2015), but over a rather small

176 area (1 × 1 m), which does not allow analyzing the multiscale nature of SSR
177 (Verhoest et al., 2008). Then, there are studies that applied one single technique,
178 but considered different SSR conditions (Taconet and Ciarletti, 2007; Marzahn et
179 al., 2012a; Gilliot et al., 2017). However, more studies carried out in large plots
180 (> 10-20 m^2) considering different measurements techniques and soil roughness
181 conditions (e.g., different tillage) are still needed for a complete understanding of
182 SSR. More precisely, the transition from profilometer based SSR measurements
183 (the standard measurement technique in the past) to 3D measurements obtained
184 from TLS or SfM photogrammetry surveys need to be explored over different SSR
185 conditions and a large plot size. This is important to evaluate the suitability of the
186 new techniques, and to be able to interpret different roughness studies performed
187 in the past.
188 Therefore, in this study, terrestrial laser scanner (TLS) and Structure from Motion
189 (SfM) photogrammetry 3D measurements were evaluated and compared with
190 laser profilometer 2D measurements obtained on three experimental 5 × 5 m SSR
191 plots tilled with different tillage implements. The objective of this work was to
192 evaluate the TLS and SfM photogrammetry techniques and to assess their
193 suitability for quantifying surface roughness in different agricultural soils. With this
194 objective, an experiment was carried out where TLS and SfM photogrammetry
195 surveys were co-registered with 2D profiles obtained using a laser profilometer.
196 Differences between techniques were evaluated visually and analytically using
197 regression analysis, and next by comparing the values of some roughness
198 parameters obtained with the techniques evaluated. Then, polar plots showing
199 multi-directional roughness parameters were computed and compared between
200 TLS and SfM photogrammetry. Finally, Digital Elevation Models (DEM) obtained

with TLS and SfM photogrammetry were compared to detect areas and surface features where a mismatch existed between techniques.

Materials and methods

Study area

This study was conducted in the experimental fields at the School of Agricultural Engineers of the Public University of Navarre in Pamplona (Navarre, Spain) (42.79º N, 1.63º W). The climate is humid sub-Mediterranean with a mean annual temperature of ~13ºC and average annual precipitation of ~720 mm distributed over ~150 days. The experimental field is almost horizontal (slope < 2%) and soils have a silty-clay-loam texture (13.7% sand, 48.3% silt and 38% clay).

Three experimental plots (5 × 5 m) were created using different tillage implements, so as to represent different surface roughness conditions typical of agricultural soils (Fig. 1). Plot 1 corresponded to high roughness conditions (Moldboard Plough), Plot 2 to medium roughness (Chisel), and Plot 3 to low roughness (Moldboard Plough + Harrowed Compacted). Moldboard Plough (MP) is a primary tillage operation performed with a plough with multiple moldboards (15–20 cm depth) that break and turn over the soil, resulting in very rough surface (Fig. 1A). Chisel (CH) is also a primary tillage operation that breaks and shatters the soil leaving it rough with residue on the surface, yet not as rough as MP (Fig. 1B). Moldboard Plough + Harrowed Compacted (HC) consists of an MP operation followed by a secondary operation using a spike harrow and a compacting roller, leading to a smooth soil (Fig. 1C).

Fig. 1. Experimental plots: (A) Moldboard Plough, (B) Chisel and (C) Moldboard Plough + Harrowed Compacted.

Experimental protocol

The data collection was carried out over three days, November 25-27 2013, where no precipitation was recorded. Profilometer measurements (Fig. 2A) were performed on November 25 afternoon in Plot 2 (CH), and on November 26 afternoon in Plot 3 (HC) and Plot 1 (MP). On each plot, eight profiles were measured, four in parallel to the tillage direction and four in perpendicular. The beginning and end points of each profile were marked with nails and referenced using a total station. To avoid the influence of sunlight shadows caused by aggregates, the acquisition of photographs for the SfM photogrammetry technique was made on November 26 later in the afternoon without direct sunlight. Twenty four photographs were taken per plot from different points-of-view using a lifting platform (Fig. 2B). Eight surveying targets were spatially distributed around the experimental plots for referencing the data. Finally, TLS measurements (Fig. 2C) were carried out on the morning of November 27. Four scans were measured per plot (i.e., one from each side), which were co-registered using five reference spheres deployed around the plots. A detailed description of the three techniques is given below.

Fig. 2. Measurement techniques: (A) Laser profilometer (PRO), (B) Structure for Motion (SfM) photogrammetry and (C) Terrestrial Laser Scanner (TLS).

Measuring techniques

Laser profilometer (PRO)

Profiles were taken with a laser profilometer (Fig. 2A) designed specifically for measuring roughness (Álvarez-Mozos et al., 2009). The device consists of a laser distance meter located inside a case that moves along an aluminum beam (fixed with two tripods) propelled by a small electric motor. The position of the carriage is measured by a rack and cogwheel mechanism on the carriage that activates a photoelectric sensor. The profilometer measures the vertical distance to the soil surface using a 3-mm wide laser beam and resamples height records to 5 mm. The laser sensor is a SICK DME 2000 with a specified vertical accuracy of 1 mm (SICK, 1996). The verticality of the laser beam is adjusted using a hand level to secure transversal and longitudinal horizontality. For each experimental plot, 5-m-long eight profiles (four parallel to the tillage direction and four perpendicular to it) were measured with the laser profilometer (Fig. 3), resulting in a total of 24 profiles.

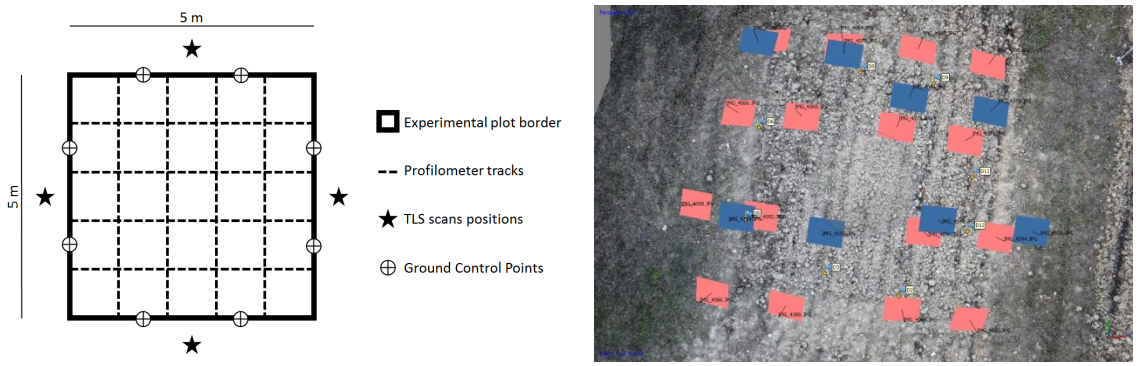

Fig. 3. Experimental setup with the approximate locations of the different measurement elements (left) and camera positions (~6 m high for red ones and ~8 m high for blue ones) calculated by PhotoScan for CH plot (right).

Profilometer data processing was done in three steps: (1) correction of the aluminum beam bending using a lab determined parabolic function, (2) outlier filtering by deleting and interpolating records larger than a threshold (i.e., 2 cm) with the previous and following records (to filter out vegetation elements eventually present on the soil surface), and (3) terrain slope correction (i.e., profile detrending) subtracting the linear trend observed in the data, if any.

The laser profilometer was considered a benchmark for 2D roughness measurements for several reasons: (1) its vertical accuracy is high; (2) its nadir-looking geometry avoids occlusions, and; (3) although it measures 2D profiles and not 3D surfaces, it has been the standard technique to characterize surface roughness for different applications for the last decades (Oh et al., 1992; Helming et al., 1998; Davidson et al., 2000; Darboux and Huang 2003; Callens et al., 2006; Verhoest et al., 2008; Baghdadi et al., 2008) and is still used at present (Zribi et al., 2019; El Hajj et al., 2019). Thus, it can be considered a state of the art technology in the field of surface roughness measurement.

291 Terrestrial Laser Scanner (TLS)

292 The TLS used in this study was the FARO Focus 3D (Fig. 2C). The scanner emits
293 a single pulse of laser light and measures the time for the reflected light between
294 the target and the scanner. The scans were obtained from a tripod ~1.75 m high.
295 The TLS has a specific ranging accuracy of 2 mm (at a distance of 25 m) and a
296 laser beam divergence of 0.16 mrad (0.009º) with a beam diameter of 3 mm (at
297 the exit) (FARO, 2018). The scan vertical and horizontal resolution was set to
298 0.018º (20480 3D pixel in 360º), so for a range distance of 6 m (maximum
299 distance in our measurements), a theoretical horizontal sampling interval of 1.84
300 mm and vertical sampling interval of 6.13 mm were obtained. For each of the
301 three experimental plots, four scans were measured (i.e., one from each side of
302 the plot) (Fig. 3).

303 For TLS data processing, raw scans were first filtered to exclude mixed-pixels
304 (points whose footprint partly includes the edge of one object and the objects
305 behind), and then, co-registered and merged into a single point cloud. The
306 filtering of mixed-pixels was performed using a self-implemented algorithm as the
307 existing predefined filters in the manufacturer software did not provide
308 satisfactory results for our data. This filtering algorithm to exclude mixed-pixels
309 was based on the incidence angle and the intensity. In this way, depending on
310 the sensor-point distance range (related to the incidence angle) intensity
311 thresholds were set to filter mixed-pixels, since they usually have low intensity
312 returns. The co-registration of individual TLS scans was done globally and using
313 the iterative closest point (ICP) algorithm implemented in the OPALS software
314 (Otepka et al., 2013; Pfeifer et al., 2014). The ICP algorithm minimizes point-to-
315 plane distances between the corresponding points (Glira et al., 2015). The quality

316 of the co-registration was assessed using the standard deviation, based on more
317 than 5000 residuals, which was about 1.1 mm for the CH and HC plots. For the
318 MP plot, the standard deviation was slightly higher (i.e., 2.5 mm) but nevertheless
319 sufficiently precise considering the specific ranging accuracy of the TLS (2 mm)
320 and that the products to be obtained for the roughness parameters analysis were
321 profiles and DEMs at 5 mm resolution. Finally, for each 5 × 5 m experimental plot,
322 a ~30 million point cloud was obtained by merging the individual co-registered
323 TLS scans per plot (see details in Table 2 and Fig. 4).

324

325 **Table 2.** Details of the data after pre-processing.

Plot	Measurement technique	No of samplings	No of readings
MP	Profilometer (PRO)	08 profiles	8,008 points*
MP	Terrestrial Laser Scanner (TLS)	04 scans	30,447,219 points
MP	Structure from Motion (SfM)	24 photos	17,303,166 points**
CH	Profilometer (PRO)	08 profiles	8,008 points*
CH	Terrestrial Laser Scanner (TLS)	04 scans	26,513,592 points
CH	Structure from Motion (SfM)	24 photos	13,507,994 points**
HC	Profilometer (PRO)	08 profiles	8,008 points*
HC	Terrestrial Laser Scanner (TLS)	04 scans	31,964,773 points
HC	Structure from Motion (SfM)	24 photos	11,548,505 points**

326 * corresponds to eight 5-m-long profiles
327 ** total points obtained from the dense point cloud
328

329 Structure from Motion (SfM) photogrammetry

330 Structure from Motion (SfM) photogrammetry is based on a set of overlapping
331 photographs acquired from different points-of-view using a high-quality digital
332 camera, which are processed automatically to determine the scene geometry and
333 camera parameters (Favally et al., 2012; Gilliot et al., 2017). For each plot 24
334 photos of 20 megapixels (5000 × 4000 pixels) were acquired with a Canon EOS
335 5D Mark II camera with a 21 mm objective Zeiss Distagon T* 2.8/21 ZE (see Fig.
336 2B). Photo acquisition was carried out with an ISO 100 speed index (sensibility)
337 and a variable aperture (~f/4) and exposure time (1/60-1/80 s) in order to adapt

to the small variations of luminosity. Photo acquisition locations were homogenously distributed (Fig. 3) and obtained from a height of ~6-8 m above ground using a lifting platform, thus capturing the entire experimental plot from each photo (100% overlapping) with a pseudo-nadir perspective. In addition, it was essential not to modify the original surface roughness of each plot, which prevented us from obtaining photos from within the plot. The spatial extent of the photos was slightly higher than the experimental plot extent, obtaining a mean pixel size of < 2 mm.

For SfM photogrammetry data processing, eight ground control points (GCP) (i.e., two on each side of the plot) were measured per plot with a total station and used for referencing the photos (Fig. 3), obtaining mean geometric error values lower than 2 mm for each plot (1.97 mm for MP class, 1.43 mm for CH and 1.14 mm for HC). Also, the errors obtained for the three axes (dX, dY, dZ) were analyzed and no spatial dependence was observed. The dense point cloud generation was done in “ultra-high quality” and “mild filtering" (in order to obtain small details) mode using the Agisoft Photoscan software (Agisoft, 2018). After this process, final point clouds were obtained with an average point spacing of ~1.7 mm on a flat surface (i.e., planimetric distance) corresponding to a minimum of 10 million points for each experimental plot (see details in Table 2 and Fig. 4).

Roughness parameters

In total, six roughness parameters were analyzed (Table 3). These parameters were selected after a previous analysis (Martinez-Agirre et al., 2016), where their correlation and their ability to discriminate between different tillage classes were assessed. All the parameters were calculated after terrain slope correction (by

363 subtracting a linear regression equation from the measured surface) (Xingming
364 et al., 2014) and height normalization for each profile (by setting the mean height
365 of the profile to 0.0) (Martinez-Agirre et al., 2016).

366

367 **Table 3.** Summary of roughness parameters analyzed.

Parameter	Description	Reference
s (cm)	Standard deviation of the heights	Allmaras et al., 1966
l (cm)	Correlation length	Ulaby et al., 1982
ρ'(0)	Initial slope of the auto-correlation function	Ulaby et al., 1982
F (cm^{-1})	Peak frequency	Römkens and Wang, 1986
T_S	Tortuosity	Saleh et al., 1993
D	Fractal dimension	Vidal Vázquez et al., 2005

368
369

370 The standard deviation of heights (*s*) (Eq. 1) is a descriptor of the vertical
371 roughness component.

372

373 $$s = \sqrt{\frac{\sum_{i=1}^{N}(z_i{}^2 - \bar{z}^2)}{N-1}} \quad (1)$$

374

375 where N is the number of the records registered in the profile, z_i is the height
376 corresponding to record i, and $\bar{z}$ is the mean height of all the records. The
377 correlation length (*l*) represents the horizontal component of roughness and is
378 defined as the distance at which the heights of two points on the surface are
379 considered independent. The correlation length is obtained from the
380 autocorrelation function (Eq. 2) (Ulaby et al., 1982):

381

382 $$\rho(h) = \frac{\sum_{i=1}^{N(h)} z_i z_{i+h}}{\sum_{i=1}^{N} z_i{}^2} \quad (2)$$

383

where $\rho(h)$ is the autocorrelation function, representing the correlation existing between the height of point *i* (z_i) and that of another point located at a lag distance *h* from it (z_{i+h}), and $N(h)$ is the number of pairs considered in each lag *h*. The correlation length (*l*) is then defined as the distance at which $\rho(h)$ is equal to $1/e$, so that $\rho(l) = 1/e$ (Euler's number (*e*) ~ 2.71828). The initial slope of the autocorrelation function (*ρ'(0)*) characterizes the horizontal component of roughness focusing on the height variations of a point with its nearest neighbors. The peak frequency (*F*) describes the horizontal component of roughness as the number of peaks (i.e., points with higher elevations than their neighbors on both sides) per unit length of the profile (Römkens and Wang, 1986). The tortuosity index of Saleh (T_S) (Eq. 3) is the ratio of the perimeter length of a profile (L_1) and its projected distance on a horizontal surface taken as reference (L_0) (Saleh et al., 1993):

$$T_S = 100 \cdot \frac{(L_1 - L_0)}{L_1} \quad (3)$$

Finally, the fractal dimension (*D*) represents the self-affinity of surface roughness profiles. In this study, the semivariogram method was used (Vidal Vázquez et al., 2005), which represents how height data are related to distance, where the semivariance function depending on the lag *h* can be calculated as in Eq. 4.

$$\gamma(h) = \frac{1}{2N(h)} \sum_{i=1}^{N(h)} [z_{i+h} - z_i]^2 \quad (4)$$

Assuming a fractal Brownian motion (*fBm*) model, the experimental semivariogram can be described as a function of the lag (Eq. 5):

$$\gamma(h) = l^{1-H} h^{H} \quad (5)$$

where *l* is the crossover length and *H* is the Hurst coefficient. After a log-log transformation, *H* is estimated as the slope of the semivariance versus the lag distance. Afterward, the fractal dimension is obtained from the Hurst coefficient as *D* = *2* - *H* (Smith, 2014).

Data analysis

The analysis presented here focused on the suitability of different measurement techniques for surface roughness parameterization in agricultural soils. For doing so, data needed to be processed to ensure that different measurements were comparable (i.e., profile length and sampling interval). First, the point clouds (for each experimental plot) obtained with TLS and SfM photogrammetry were co-registered to the same reference system using the ICP algorithm implemented in OPALS. The standard deviation obtained of the point-to-plane residuals was less than 2 mm for the three plots (this value was based on more than 1000 correspondences). Next, profiles were extracted from the TLS and SfM photogrammetry point clouds coinciding with the location of the profiles measured with the profilometer. The extraction of these profiles was done to imitate the profilometer measurement principle. First, all the points of the cloud closer than 1.5 mm (comparable to the laser beam size (3 mm) of the profilometer) to the profile centerline were selected from the TLS and SfM photogrammetry point clouds. Then, these points were (1) processed to avoid occlusions (i.e., hollow spaces) in order to obtain just one height data for every profile length; (2) binned

434 at bin intervals of 5 mm to resemble the measurement interval of the profilometer;
435 and (3) interpolated to avoid empty data (shadowed regions). Finally, profiles
436 were limited to 4-m-long in order to avoid surface roughness modifications in the
437 beginning and the end of the profiles.
438 Measurement techniques were compared in two steps. First, a comparison based
439 on 2D roughness data (i.e., profiles) was performed both in parallel and
440 perpendicular to the tillage direction. This comparison was made following three
441 criteria: (1) visual analysis of the profiles obtained with the different techniques;
442 (2) analytical comparison of the profiles using scatterplots, regression analysis
443 and RMSE estimation, and special dependence analysis; and (3) evaluation in
444 terms of the roughness parameters values extracted from the profiles. To analyze
445 the differences between techniques, a paired t-test (Montgomery, 1991)
446 comparing roughness parameters values obtained from the profiles obtained with
447 the three techniques has been carried out. Second, a 3D roughness analysis was
448 carried out using point clouds obtained with TLS and SfM photogrammetry. Here,
449 two elements were compared: (1) multidirectional roughness parameters values
450 (using four profiles obtained in every 15º azimuth); and (2) DEM comparison
451 (where DEMs were obtained for TLS and SfM photogrammetry, respectively, by
452 computing the mean height value on the point cloud for 5 mm grid size and using
453 a linear interpolation for the empty pixels).
454
455
456 **Results**
457
458 *Point density analysis*

459 It must be taken into account that the point cloud distribution was conditioned by
460 the data acquisition geometry. In this sense, the point density of TLS was ~2
461 times higher than that of SfM photogrammetry (Table 2 and Table 4), and what
462 is more, the distribution of this point density was rather different (Fig. 4). SfM
463 photogrammetry provided a more homogeneous distribution throughout the soil
464 surface, whereas TLS (probably due to its side looking geometry) led to a higher
465 number of points at the border of the plots and around soil aggregates. This TLS
466 acquisition geometry also provided a higher point density Standard Deviation
467 (SD) (Table 4), in particular for rougher surface conditions. The difference in the
468 number of pixels without data was also remarkable (Table 4). SfM
469 photogrammetry had none empty pixels, whereas TLS had a high number due to
470 shadowing effects in the roughest surfaces (~13% in MP), although this value
471 decreased markedly for the CH and HC plots (~6% and ~2%, respectively).

472

473 **Table 4.** Mean point density per pixel (5 mm x 5 mm), Standard Deviation (SD)
474 and proportion of pixels without data (%) for the different plots obtained by TLS
475 and SfM photogrammetry techniques.

Technique	Plot	Mean (p/pixel)	SD (p/pixel)	No data (%)
TLS	MP	30.3	33.1	13.48
	CH	24.3	24.0	5.83
	HC	29.4	22.0	1.56
SfM	MP	17.2	8.0	0
	CH	12.4	4.7	0
	HC	10.6	3.0	0

476

477

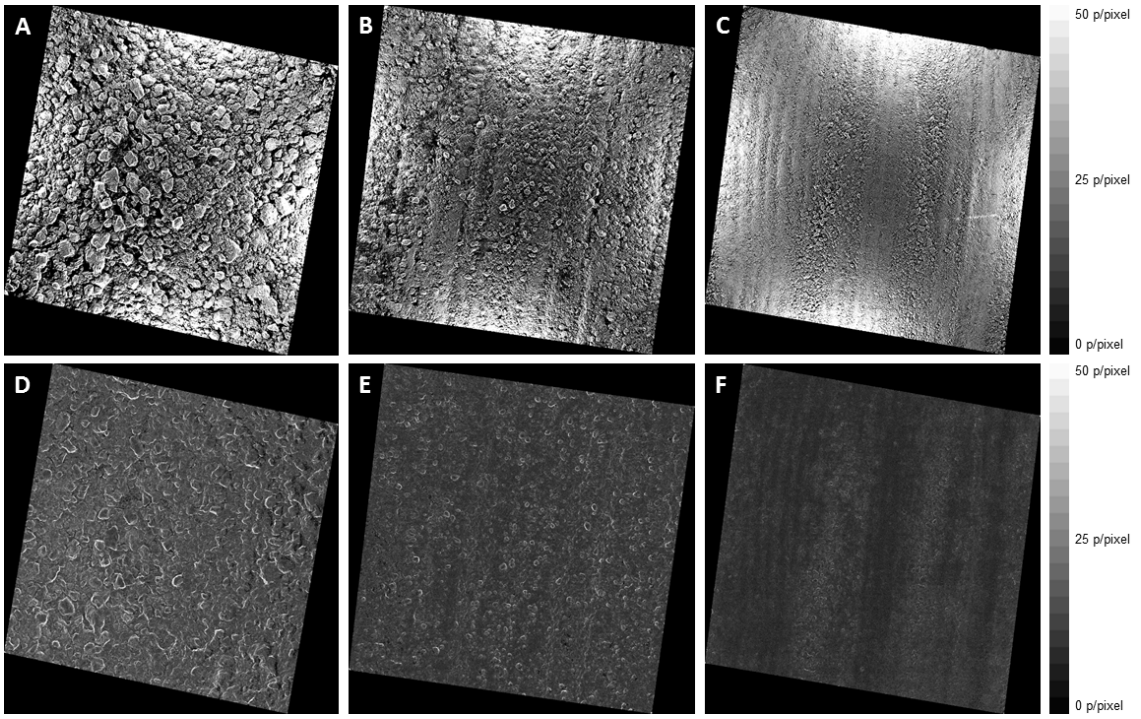

Fig. 4. Mean point density per pixel (for a 5x5 mm grid) obtained with TLS technique for MP plot (A), CH plot (B) and HC plot (C), and obtained with SfM photogrammetry technique for MP plot (D), CH plot (E) and HC plot (F).

Visual analysis

A first visual exploration of the same profiles obtained with the three techniques revealed interesting details (Fig. 5). Although, the analyzed profiles generally showed very similar geometries, some differences were noticed, particularly in the roughest classes (MP and CH). Both TLS and SfM photogrammetry resulted in smoothed profiles when compared to the profilometer (PRO), with SfM photogrammetry yielding the smoothest profiles (Fig. 5). Profiles obtained from both techniques were unable to accurately describe sudden elevation changes (both positive and negative) typical at the edges of soil clods and larger aggregates (Fig. 5). In the CH and HC classes, the agreement was higher, but

still, some slight differences were observed when height variations occurred at small distances (Fig. 5).

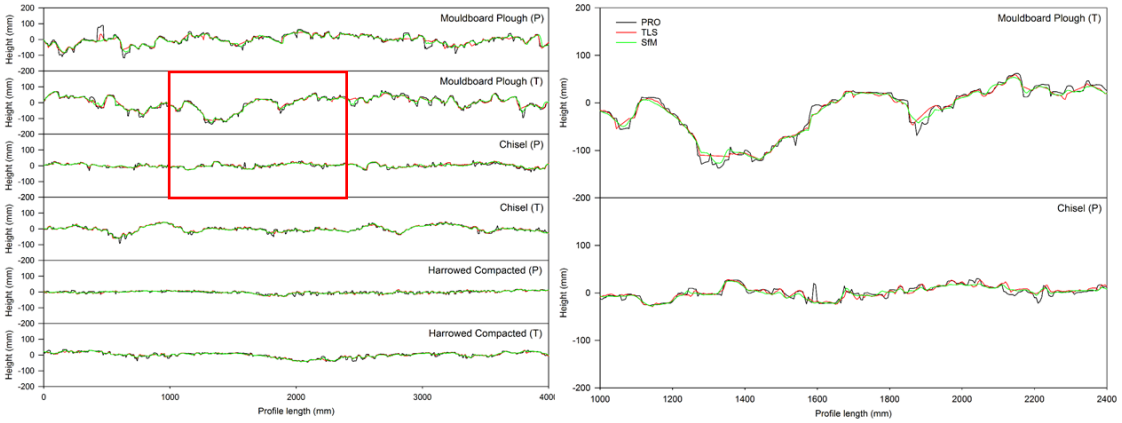

Fig. 5. Example height profiles of the different roughness classes in parallel (P) and perpendicular (T) to the tillage direction obtained with the different measurement techniques. The right panel is a zoomed version of the detail zone drawn with the red rectangle.

Scatterplot analysis

Scatterplots representing the height of each point of the profiles obtained with the different techniques were represented for each roughness class and direction (parallel and perpendicular to the tillage) (Fig. 6-8). For each scatterplot, a linear regression was fitted, and the agreement between techniques was evaluated by means of the root mean square error (RMSE) and the coefficient of determination (R^2).

In the MP roughness class (Fig. 6), TLS and SfM photogrammetry techniques had a good agreement with the profilometer (PRO) in both parallel (Fig. 6A-B) and perpendicular (Fig. 6D-E) to the tillage direction. However, they agreed better (higher R^2 and lower RMSE) in the perpendicular direction (RMSE ~13 mm and

513 R^2 ~0.9) (Fig. 6D-E) than in parallel (RMSE ~20 mm and R^2 ~0.7) (Fig. 6A-B).
514 When comparing TLS and SfM photogrammetry, RMSE decreased and R^2
515 increased, especially in the perpendicular direction (R^2 > 0.95) (Fig. 6F).
516 However, in parallel (Fig. 6C) to tillage, some disagreement appeared in medium-
517 high elevation values of TLS and in medium-low of SfM photogrammetry, which
518 could represent interpolated TLS data in shadowed regions.
519 In the CH roughness class (Fig. 7), the differences between TLS and SfM
520 photogrammetry with PRO were lower than in the MP class, with values of ~7
521 mm in the parallel direction (Fig. 7A-B) and ~8 mm in perpendicular (Fig. 7D-E).
522 Also, the goodness-of-fit between the TLS and SfM photogrammetry techniques
523 was higher with a lower RMSE (~5 mm) and higher correlation than in MP (Fig.
524 7C and 7F), especially in the perpendicular direction (R^2 ~0.95) (Fig. 7F). In this
525 case, the number of outliers was lower than in the MP class.
526 The HC roughness class (Fig. 8) presented the lowest differences between TLS
527 and SfM photogrammetry with PRO, yielding RMSE values ~5 mm in both
528 directions (Fig. 8A-B and 8D-E). Also, the values between TLS and SfM
529 photogrammetry presented the best fit with an RMSE of ~3 mm and high
530 correlation and slope values (Fig. 8C and 8F), especially in the perpendicular
531 direction (slope and R^2 > 0.95) (Fig. 8F). In this case, the presence of
532 disagreement was almost null.

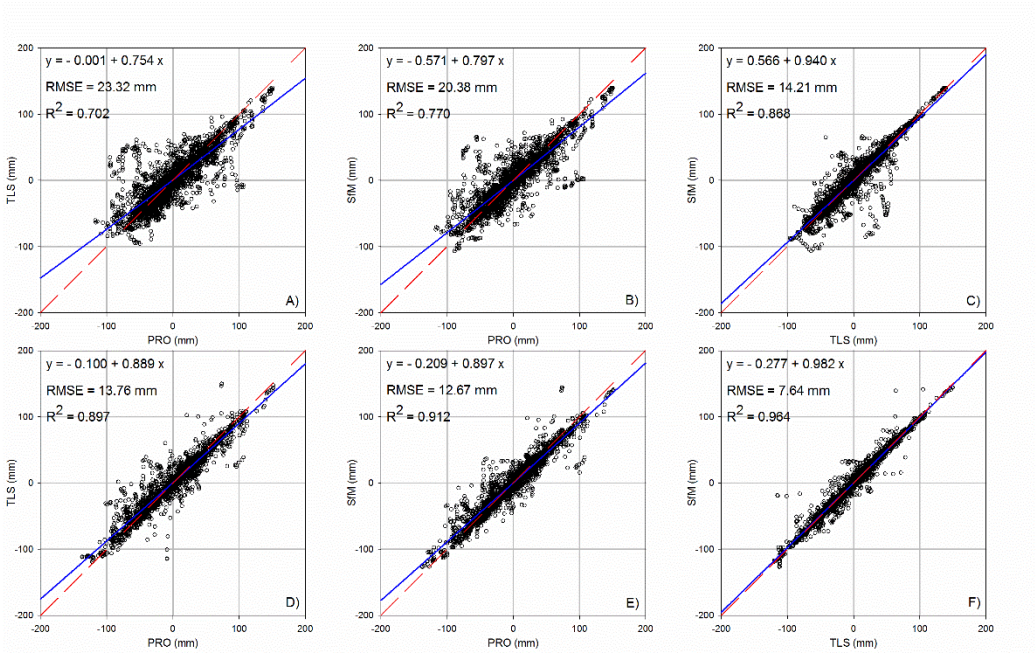

533

534 **Fig. 6.** Scatter-plots of profile heights acquired using different measurement
535 techniques for Moldboard Plough (MP) class in parallel (top) and perpendicular
536 (bottom) to the tillage direction. Dotted line (red) represents the identity (1:1) line
537 and solid line (blue) represents the linear regression.

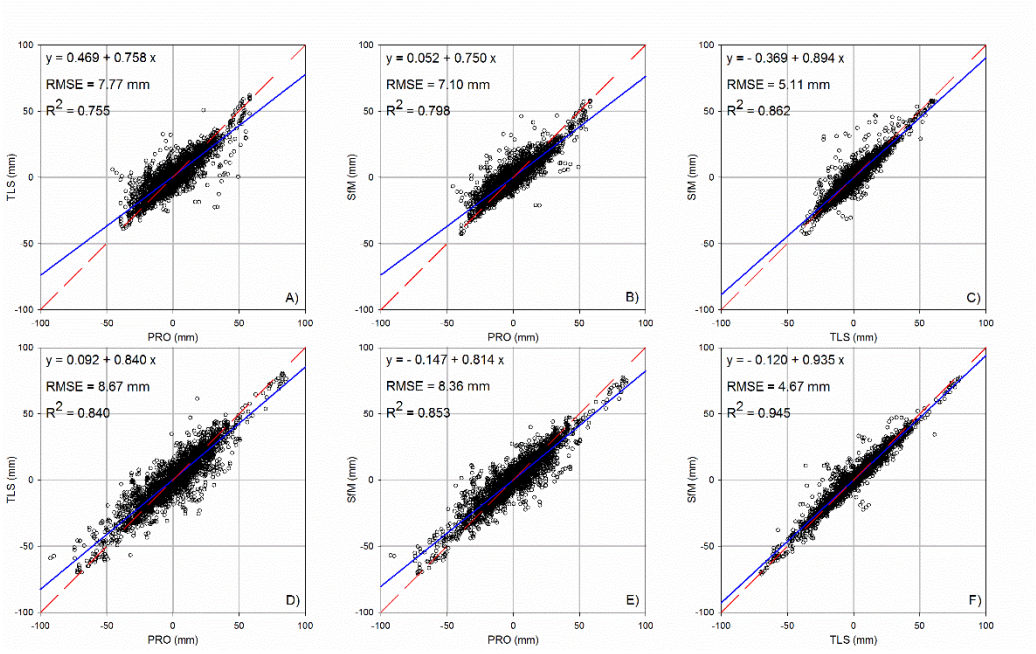

538

539 **Fig. 7.** Scatter-plots of profile heights acquired using different measurement
540 techniques for Chisel (CH) class in parallel (top) and perpendicular (bottom) to

541 the tillage direction. Dotted line (red) represents the identity (1:1) line and solid
542 line (blue) represents the linear regression.

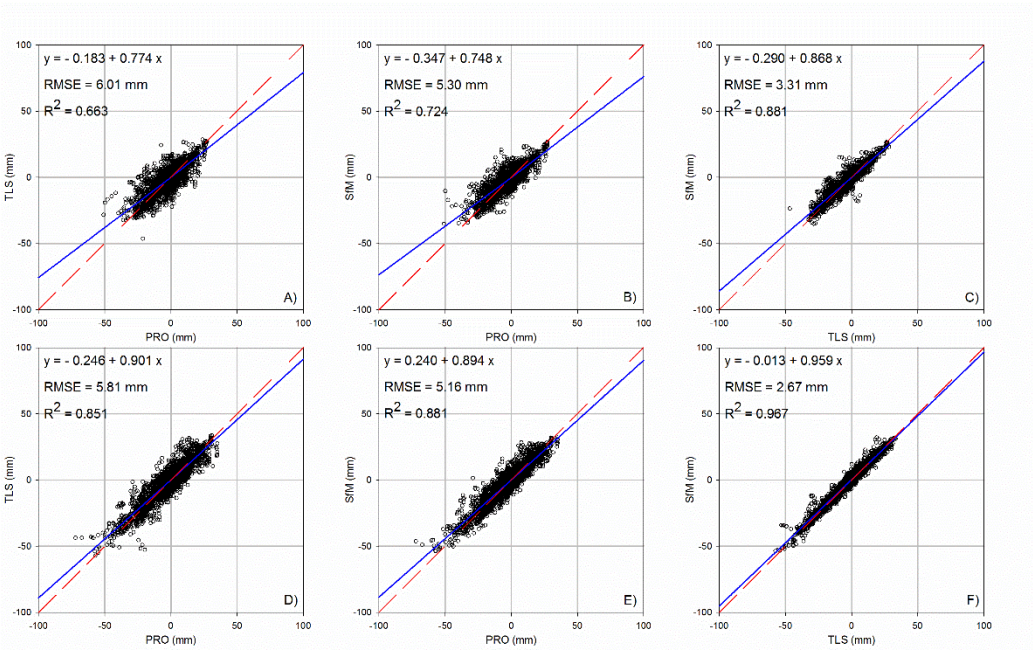

543

544 **Fig. 8.** Scatter-plots of profile heights acquired using different measurement
545 techniques for Harrowed Compacted (HC) class in parallel (top) and
546 perpendicular (bottom) to the tillage direction. Dotted line (red) represents the
547 identity (1:1) line and solid line (blue) represents the linear regression.

548

549 To analyze any possible spatial dependence (i.e., systematic error propagation)
550 between profiles obtained with the different techniques, the mean RMSE in
551 segments of 5 height records (i.e., 25 mm) between the profiles obtained with the
552 different techniques for each experimental plot was carried out (Fig. 9). In
553 general, the spatial dependence analysis confirmed the results observed in the
554 scatterplots (Fig. 6-8). However, it should be noted that in TLS-SfM and PRO-
555 SfM a small spatial dependence was observed (especially in rougher plots),
556 slightly increasing the RMSE at the edges of the profiles.

557

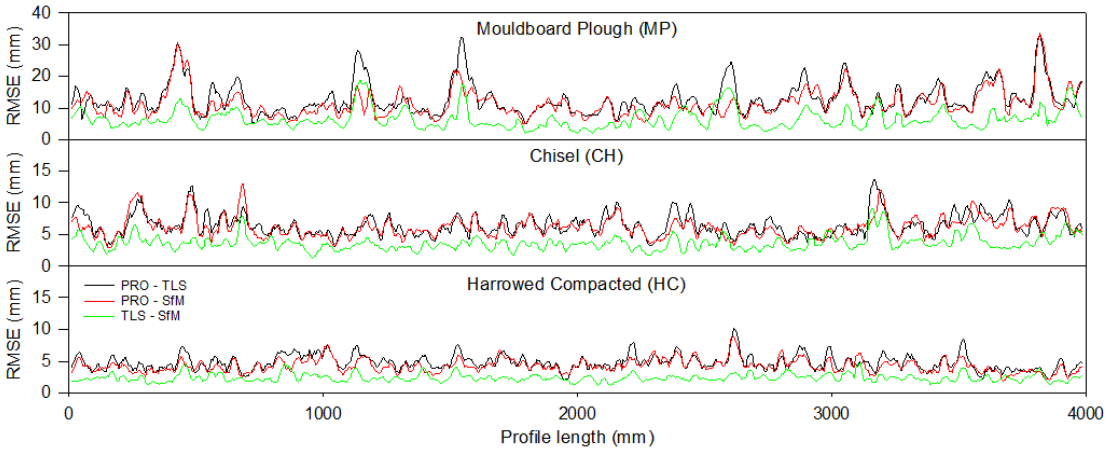

Fig. 9. Mean RMSE in segments of 5 height records (25 mm) between the profiles (n=8) obtained with the different techniques for each plot.

Roughness parameters analysis

Figure 10 presents the mean values and standard deviations of the roughness parameters obtained with the three techniques for each experimental plot and measurement direction. The standard deviation of heights (*s*) showed very similar class mean values and standard deviations for the three techniques analyzed (Fig. 10A). However, PRO presented slightly higher values followed by TLS and SfM photogrammetry. The difference in MP roughness class between the TLS and SfM photogrammetry technique was inappreciable. As expected, the MP class presented higher values followed by CH and HC, and also the perpendicular (T) direction showed higher values than the parallel (P) direction. The correlation length (*l*) presented a different behavior with lower values (and deviations) for CH class, followed by MP and HC (with higher values and especially larger deviations), and the perpendicular direction also showed higher values than the parallel direction (Fig. 10B). Regarding the different techniques, in general, PRO showed the lowest values followed by TLS and SfM photogrammetry. The initial

577 slope of the autocorrelation function ($\rho'(0)$), although being similar to l in concept,
578 presented a very different behavior, with higher values for the HC class, followed
579 by CH and MP and higher values in parallel than in perpendicular (Fig. 10C). The
580 differences between the measurement techniques were higher than in any other
581 parameter evaluated with higher values for PRO followed by TLS and SfM
582 photogrammetry.
583 The tortuosity (T_S) showed higher values for PRO followed by TLS and SfM
584 photogrammetry, and also higher values for the MP class followed by CH and HC
585 (Fig. 10D). However, no remarkable differences were appreciated between the
586 parallel and perpendicular directions. The peak frequency (F) took higher values
587 for PRO or TLS depending on the roughness class and lower values for SfM
588 photogrammetry (Fig. 10E). In general, the MP class showed lower values
589 followed by CH and HC (except for PRO technique) and no remarkable
590 differences were observed between parallel and perpendicular directions. The
591 fractal dimension (D) behaved similarly, with higher values for PRO followed by
592 TLS and SfM photogrammetry, lower values for the MP roughness class followed
593 by CH and HC, and with no important differences between the parallel and
594 perpendicular directions (Fig. 10F).
595

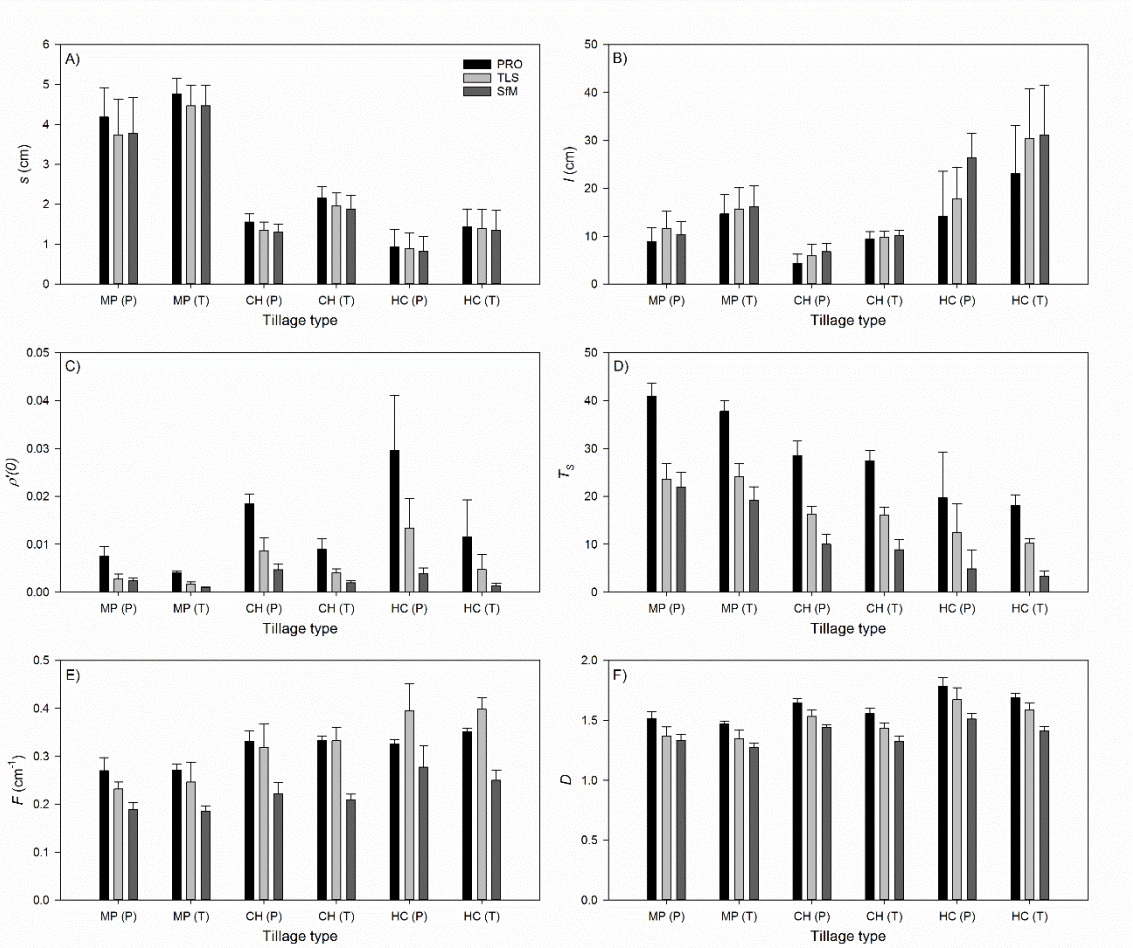

Fig. 10. Roughness parameters values for the different measurement techniques and for the different roughness classes analyzed: Moldboard Plough (MP), Chisel (CH) and Harrowed Compacted (HC), in parallel (P) and perpendicular (T) to tillage direction.

Statistically (Table 5), Significant differences were observed in all cases except for the peak frequency (*F*) parameter measured with PRO and TLS (p-value > 0.05), the correlation length (*l*) measured by TLS and SfM photogrammetry (p-value > 0.01) and with PRO and TLS (p-value > 0.001), and the standard deviation of heights (*s*) measured by TLS and SfM photogrammetry (p-value > 0.001). Regarding the mean relative differences (%) obtained for each parameter, differences between PRO and SfM photogrammetry were the highest ones,

609 followed by PRO-TLS and TLS-SfM photogrammetry (with the exception of the
610 peak frequency (*F*)).

611

612 **Table 5.** Paired t-test of the different techniques. Mean relative differences (%)
613 and p-values obtained for the different roughness parameters. No asterisks
614 implies significant differences.

Paired techniques	*s*	*l*	*ρ'(0)*	*F*	T_S	*D*
PRO – TLS	7.9	-30.8*	57.4	-1.8***	40.7	7.5
PRO – SfM	11.0	-50.3	77.8	29.1	65.5	14.0
TLS – SfM	3.1*	-14.2**	44.4	29.6	40.7	6.8

615 * p-value > 0.001
616 ** p-value > 0.01
617 *** p-value > 0.05
618

619 To analyze the high-frequency roughness, mean autocorrelation functions were
620 visualized for the different measurement techniques (Fig. 11). In all roughness
621 conditions and both directions (except MP in parallel), PRO showed lower *l* and
622 higher *ρ'(0)* values, followed by TLS and SfM photogrammetry. The mean
623 autocorrelation functions showed that for HC (P) SfM photogrammetry had the
624 most smoothened profiles (i.e., higher autocorrelation values), whereas for MP
625 (P) TLS was actually more smoothened than SfM photogrammetry, but only for
626 spatial lags shorter than 400 mm. In this way, it could be confirmed that profiles
627 obtained from TLS and especially SfM photogrammetry presented lower high-
628 frequency roughness information (i.e., smoothing) when compared to the profiles
629 obtained with PRO.

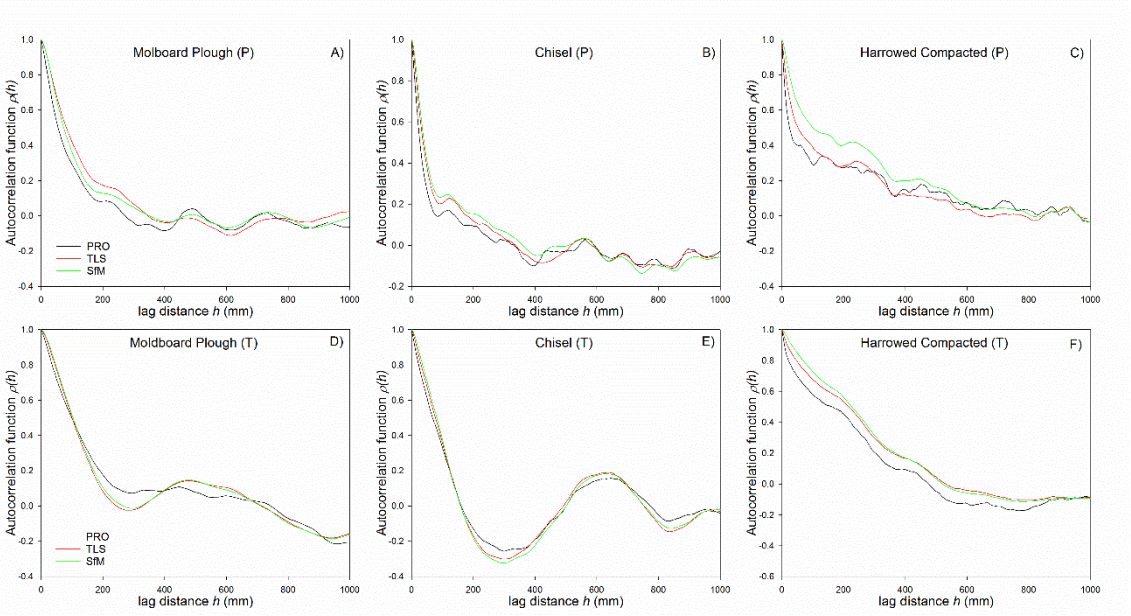

630

631 **Fig. 11.** Mean autocorrelation function for the different measurement techniques
632 and for the different roughness classes in parallel (P) and perpendicular (T) to
633 tillage direction.

634

635 *Multi directional roughness parameter analysis*

636 To analyze the multidirectional behavior of roughness parameters with TLS and
637 SfM photogrammetry techniques, polar plots were used to represent mean values
638 of the roughness parameters. For the MP roughness class (Fig. 12), *s* showed a
639 similar behavior for both techniques (with little exceptions), with higher values at
640 the 90º direction (i.e., perpendicular to tillage). The correlation length (*l*) also
641 presented a similar behavior with both techniques, but no clear directionality was
642 observed with a rather large variability at different directions. Parameter *ρ'(0)*
643 showed differences between techniques (higher values with TLS) and a notable
644 anisotropic behavior with peak values in the 0º direction (i.e., parallel to tillage).
645 On the other hand, tortuosity (T_S) and peak frequency (*F*) presented higher values
646 for the TLS technique and no significant directional behavior. Finally, the fractal

dimension (*D*) showed almost identical values for both techniques and isotropic behavior.

Regarding the CH roughness class (Fig. 13), *s* and *l* parameters presented very similar values with both techniques. However, these showed an anisotropic behavior (especially *l*) with low values in the 0º direction and higher values in the 30º or 105º directions. Parameter $\rho'(0)$ presented higher values with TLS and a strong anisotropic behavior with higher values in the 0º direction. Finally, parameters T_S, *F*, and *D* showed clear differences with higher values obtained for TLS (only slight differences in *D*) and no significant directional behavior.

For the HC roughness class (Fig. 14), the *s* parameter presented similar values with both techniques and an anisotropic behavior with lower values in the near parallel directions. The parameter *l* showed little differences with higher values for the SfM photogrammetry technique (especially in some directions) and a clear anisotropic behavior with lower values in the near parallel directions. Parameter $\rho'(0)$ presented clear differences with higher values observed for TLS and a strong directional behavior with highest values in the 0º direction. Finally, parameters T_S, *F*, and *D* showed large differences with higher values for the TLS technique (fewer differences in *D*) and isotropic behavior (except T_S with a peak in the 0º direction).

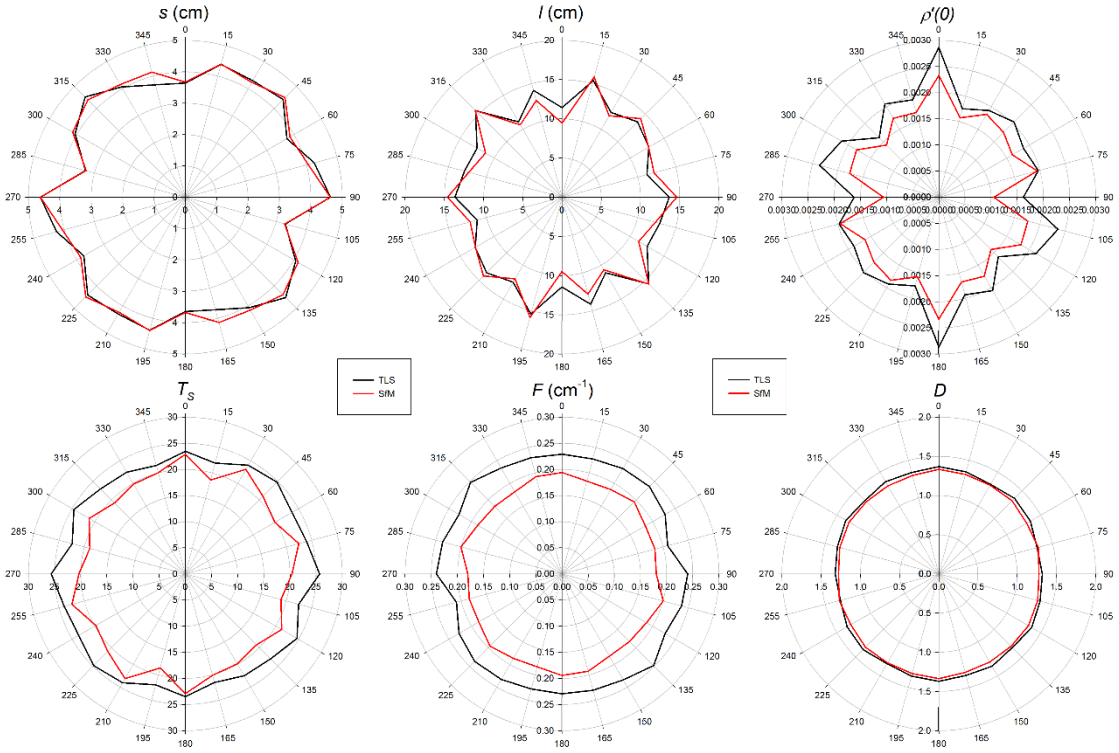

Fig. 12. Multi directional roughness parameter values from TLS and SfM photogrammetry techniques in Moldboard Plough (MP) class.

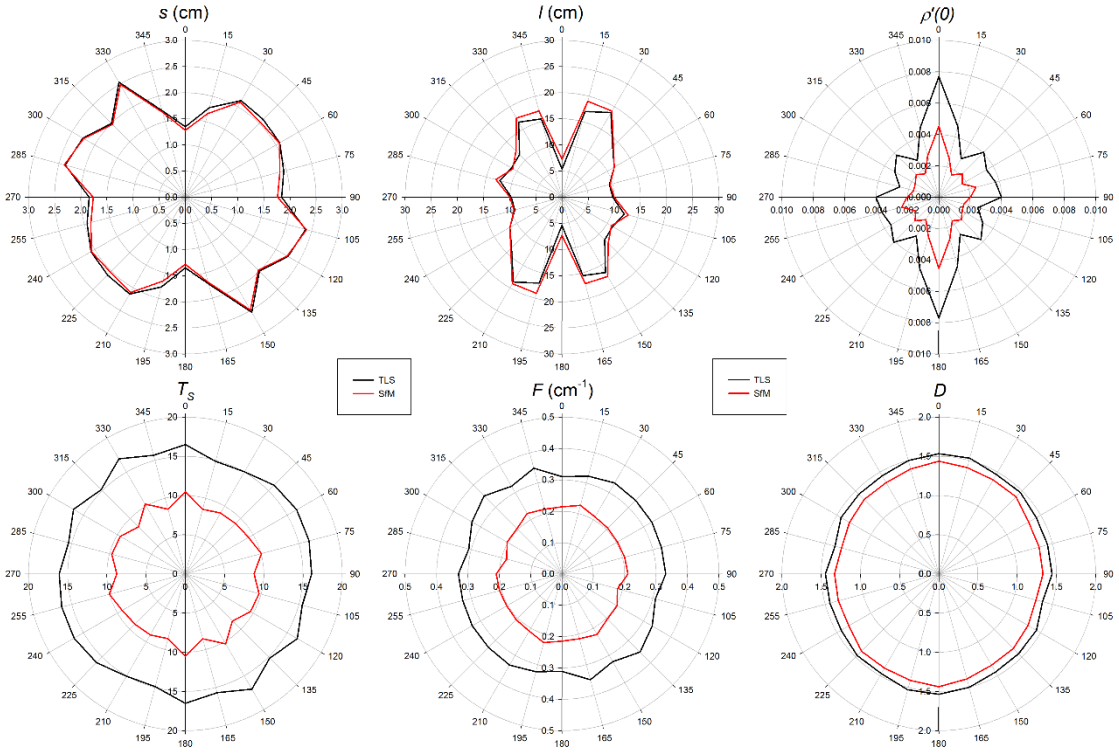

Fig. 13. Multi directional roughness parameter values from TLS and SfM photogrammetry techniques in Chisel (CH) class.

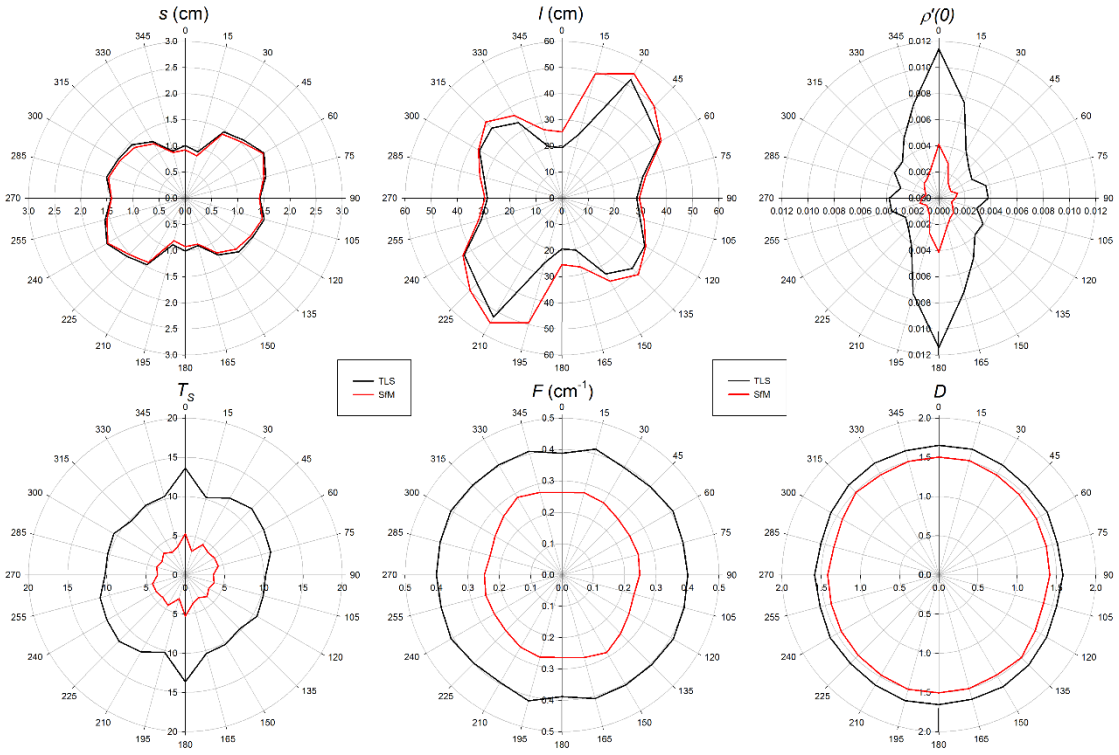

Fig. 14. Multi directional roughness parameter values from TLS and SfM photogrammetry techniques in Harrowed Compacter (HC) class.

DEM analysis

The hillshade DEMs obtained with the TLS and SfM photogrammetry techniques and their differences are shown in Figure 15. In general, DEMs obtained with TLS seemed to be more detailed than with SfM photogrammetry. This phenomenon is better appreciated in CH and HC classes where a difference in the higher frequency roughness components is apparent between TLS and SfM photogrammetry. Also, a small spatial dependence of the errors between the center (in light blue) and the edges (in light red) of the plot was observed in the

684 rougher classes (MP and CH). This confirmed what was observed in the RMSE
685 analysis of the profiles (Fig. 9).
686 Regarding the differences between roughness classes, in the MP class (Fig.
687 15C), some dark blue zones (with higher values for TLS) were observed due to
688 interpolated shadowed regions (no data) for TLS. Also, little dark red zones (with
689 higher values for SfM photogrammetry) appeared in the lower part of some
690 aggregates because of the smoothing surface behavior of SfM photogrammetry,
691 especially in the border of the plot (due to a higher zenith incidence angle for
692 TLS). In the center of the plot, a light blue color was predominant (0-5 mm), which
693 could be caused by a higher detailed geometry of the clods (medium and high
694 parts) with TLS, comparing with the surface smoothing behavior with SfM
695 photogrammetry. For the CH class (Fig. 15F), the differences were lower than in
696 MP, with just some small red zones (with higher values for SfM photogrammetry)
697 along the border of the experimental plot caused by the same phenomenon
698 explained for MP class. Finally, the differences observed in the HC class (Fig.
699 15I) were practically null.
700 It should be noted that the blue zones that appear in different corners of the three
701 experimental plots were caused by the reference spheres used for the TLS co-
702 registration.
703

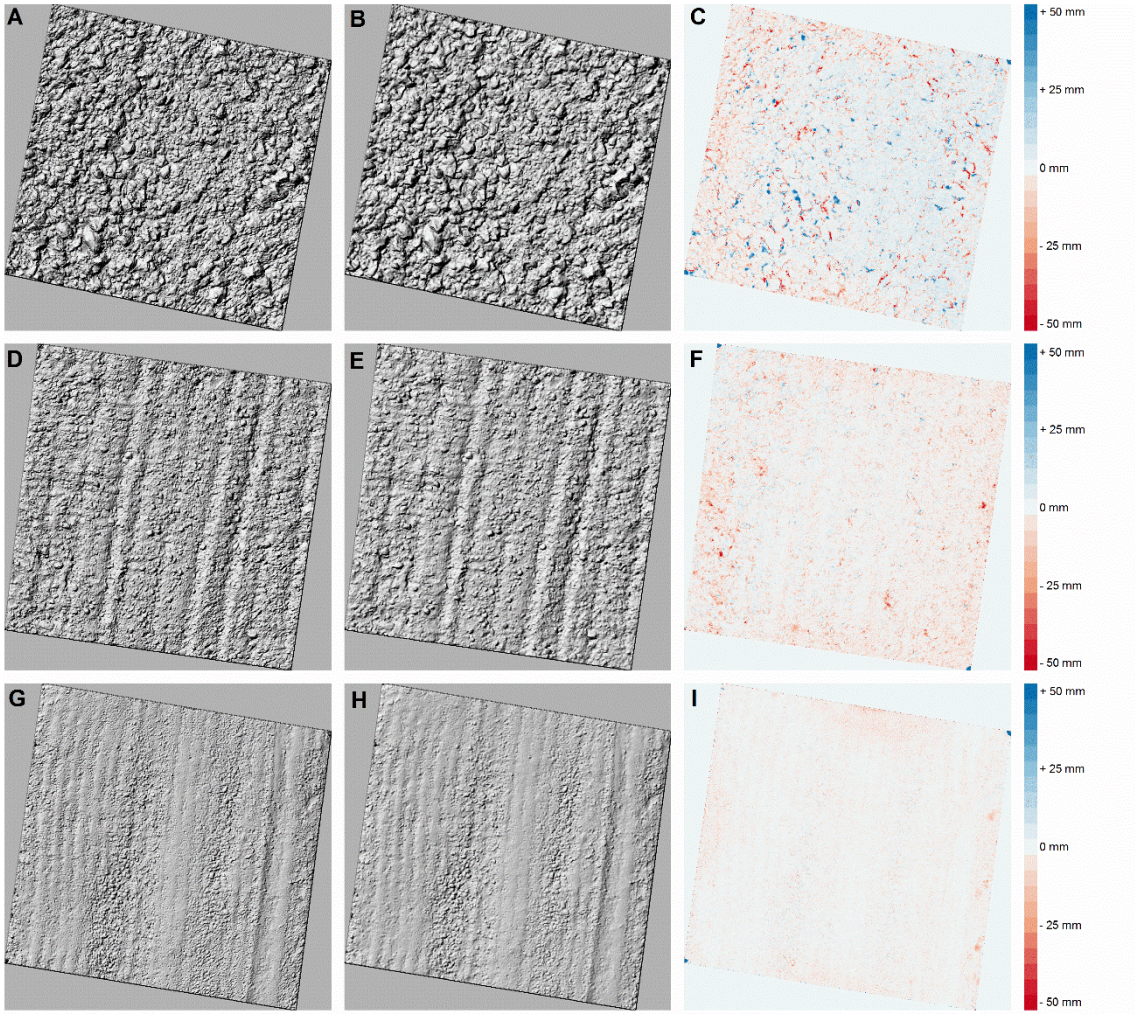

Fig. 15. Hillshade DEMs with 5 mm grid size obtained for TLS (left column) and SfM photogrammetry (center column), and their difference (TLS-SfM) (right column); for Moldboard Plough (MP) class (top), Chisel (CH) class (middle) and Harrowed Compacted (HC) class (bottom).

Discussion

The analysis performed here is unique since it considers different roughness (i.e., tillage) classes and significantly larger experimental plots than other studies on this topic. Also, it is the first time here that height profiles obtained with different

716 SSR techniques are directly compared due to the precise co-registration
717 achieved, including the profilometer, considered the standard in the past.
718 However, it must be taken into account that the analysis compares surface
719 roughness datasets obtained with the three techniques, and not the techniques
720 in absolute terms (since not all the possible variants and setting of the techniques
721 are explored, e.g., different acquisition heights for SfM photogrammetry, etc.).
722 Such an analysis should be most welcome.
723 The final point clouds obtained with the TLS and SfM photogrammetry techniques
724 had a very good correspondence. On the one hand, after SfM photogrammetry
725 referencing, GCP mean errors ranged between 1.1 mm (for HC class) and 1.9
726 mm (for MP class). These values are comparable to Bretar et al. (2013), Snapir
727 et al. (2014), and Gilliot et al. (2017), who reported errors of ~1.5 mm. On the
728 other hand, the average distance between the corresponding points among TLS
729 scans for each plot was ~1 mm (similar to Milenković et al., 2015), except for MP
730 (2.5 mm) due to a very rough terrain that imposed shadowed regions and thus
731 affected the ICP correspondences. Finally, the average distance between point
732 clouds obtained by the TLS and SfM photogrammetry techniques was less than
733 2 mm for all the three plots.
734 Regarding the bidirectional (parallel and perpendicular to tillage direction)
735 analysis of the different measurement techniques, the visual analysis provided
736 interesting information. The rougher the surface, the more evident the smoothing
737 of the profiles obtained by TLS and SfM photogrammetry techniques was with
738 respect to PRO, with profiles obtained with SfM photogrammetry yielding the
739 smoothest ones (Fig. 5 and 11). On the one hand, interpolated shadowed regions
740 in TLS due to large aggregates on the soil surface (Heng et al., 2010) caused

741 considerable differences in some parts of the profiles. Therefore, the eventual
742 availability of a nadir-looking TLS acquisition (e.g., installed on a lifting platform
743 or even on board a Remotely Piloted Aerial System) could circumvent this
744 limitation. This is not easy to achieve due to the sensing time required by TLS
745 equipment and the necessity to accurately determine the position of the sensor
746 to precisely locate the obtained point cloud. Altogether, TLS seems to provide
747 accurate height information even for high-frequency elevation variations but, with
748 the present setting (i.e., side looking surveys), the reliability of this technique is
749 affected by shadowing effects especially in rougher surfaces (MP and CH) (Table
750 4). On the other hand, it must be remarked that the resolution of laser-based
751 techniques (i.e., PRO and TLS) will have a negligible improvement by reducing
752 the distance (due to the laser beam diameter), while the resolution of SfM
753 photogrammetry will definitively improve with shorter distances (and higher
754 number of photos). In this regard, an improvement in resolution (including high-
755 frequency roughness) should be explored in the future in the application of SfM
756 photogrammetry to surface roughness studies.
757 The scatterplot analysis provided very interesting information regarding the
758 profiles co-registration obtained with the different techniques. As expected, the
759 overall adjustment between the different techniques decreased (higher RMSE
760 and lower R^2) when surface roughness increased. This fact could be due to that
761 errors in the X/Y direction have a greater effect on the deviation in Z in areas of
762 higher local slopes (i.e., rougher surfaces). The various degrees of adjustment
763 achieved between the different techniques was also remarkable. In this sense, a
764 greater adjustment (lower RMSE and higher R^2) was clearly seen between TLS
765 and SfM photogrammetry with respect to PRO. This fact seemed unexpected if

766 we consider that TLS and SfM photogrammetry are techniques based on
767 absolutely different technologies. However, it must be taken into account that the
768 methodology to extract the profiles from the point clouds was rather similar in
769 both cases. In this sense, the number of points used to calculate the height at
770 each point of the profile is a key element, being much more similar between TLS
771 and SfM photogrammetry than with PRO. At the same time, there was also a
772 slightly greater adjustment between PRO and SfM photogrammetry with respect
773 to TLS. These discrepancies in the adjustment were expected taking into account
774 the methodology used for point clouds and profiles co-registration. Both the
775 profiles obtained with PRO (the beginning and end points) and GCPs used in SfM
776 photogrammetry were referenced using a total station, while TLS point clouds
777 were co-registered (and referenced) with SfM photogrammetry point clouds using
778 the ICP algorithm. These methodological details could have impact in the results
779 obtained.
780 Regarding the roughness parameters values obtained with different techniques,
781 the slight differences for parameter *s* observed in the presented work are in
782 agreement with the harrowed and ploughed surfaces studied by Thomsen et al.
783 (2015). In this sense, for the harrowed field, they reported lower *s* values with
784 stereo-photogrammetry (-16%) than with TLS. Also, the only analysis comparing
785 laser profilometer with stereo-photogrammetry showed higher *s* values (~50%)
786 and *l* values (~20%) for the laser profilometer (Blaes and Defourny, 2008). On
787 the other hand, differences between roughness classes were clear with
788 parameter *s*, which confirmed the results of the different studies where *s* has been
789 proposed for distinguishing different roughness classes (Helming et al., 1993;
790 Magunda et al., 1997; Kamphorst et al., 2000; Vermang et al., 2013; Bauer et al.,

2015; Martinez-Agirre et al., 2016). For the horizontal parameter *l*, there is no agreement in the literature. Some authors (Davidson et al., 2003; Baghdadi et al., 2008) reported increasing values for *l* for increasing roughness conditions, while others observed similar values in different roughness classes (Álvarez-Mozos et al., 2005; Verhoest et al., 2008). This parameter has been found to be strongly dependent on the scale of measurement with large values corresponding to larger sampling intervals (Barber et al., 2016) and low-frequency roughness components (Martinez-Agirre et al., 2017). For the rest of the parameters analyzed, the general behavior with SfM photogrammetry and, to a lesser extent, with TLS was the underestimation of the different parameters values when compared to PRO.

In the multi-directional analysis, both techniques (TLS and SfM photogrammetry) agreed in the directional behavior of the different roughness parameters analyzed. Few analyses have evaluated the multi-directional behavior of roughness parameters in agricultural soils (Blaes and Defourny, 2008; Snapir et al., 2014), concluding that both *s* and especially *l* were conditioned by tillage direction. In this analysis, this phenomenon is especially relevant for $\rho'(0)$, with higher values in parallel to the tillage direction and lower values in directions near to the perpendicular, and to a lesser extent for *s* and *l* in CH and HC roughness classes. For these two parameters (especially for *l*), the highest values are obtained in oblique to the tillage direction (15º-75º or 105º-175º); this seems logical in the case of *l* since the distance between the tillage marks were greater than in perpendicular (90º). Finally, it should be noted that MP roughness class provided the most isotropic roughness, because the multiple moldboards broke and turned over the soil providing a very rough surface in all directions. The other

816 classes were indeed smoother but produced some king of a slight furrow pattern.
817 This type of information is of great interest in radar remote sensing, since it has
818 been observed that, in agricultural soils, radar backscatter could be greatly
819 affected by the directionality of the soil roughness (Wegmueller et al., 2011;
820 Marzahn et al., 2012b).
821 Regarding the DEMs obtained with TLS and SfM photogrammetry, it could be
822 said that both techniques were valid to represent the surface roughness of the
823 typical agricultural soils. Despite this, some limitations must be taken into
824 account. On the one hand, the high accuracy and resolution of TLS were limited
825 by the data acquisition geometry (scans positions), thus generating shadowed
826 regions without data, especially in the roughest soils. On the other hand, despite
827 of the good geometry of the SfM photogrammetry acquisition (from a lifting
828 platform), the generated DEMs (and also the point clouds) showed a certain
829 smoothing concerning to other techniques, which was particularly apparent when
830 horizontal roughness parameters were calculated. As mentioned previously, the
831 limitations of TLS could be avoided with a nadiral geometry, and the limitations
832 of SfM photogrammetry with a shorter acquisition distance (and a greater
833 number) of photos.
834
835
836 **Conclusions**
837
838 The results obtained demonstrate the ability of both TLS and SfM
839 photogrammetry techniques to measure surface roughness over agricultural
840 soils. This is considered relevant since the experimental setting enabled a direct

841 comparison of profiles measured with different techniques, due to the precise co-
842 registration achieved. The agreement between the elevation profiles obtained
843 with TLS and SfM photogrammetry when compared to those obtained with a
844 nadir-looking profilometer was reasonable, and RMSE values were below 10 mm
845 for smooth and intermediate roughness conditions. Rough soils (MP) were more
846 challenging and RMSE values as high as 20 mm were obtained for this class. Yet
847 these differences were not that relevant when different roughness parameters
848 were computed. Parameter *s*, and to a lesser extent *l*, showed similar values
849 when measured with the different techniques. However, some other roughness
850 parameters, more sensitive to the spatial arrangement of height variations, such
851 as $\rho'(0)$, F or T_S, showed lower of high-frequency elevation information in profiles
852 obtained from TLS and especially in SfM photogrammetry data in comparison to
853 PRO. This smoothing effect seems to be inherent to the experimental setup in
854 the case of SfM photogrammetry surveys and related to shadowed zones in the
855 TLS data due to its oblique viewing geometry. The first could be improved with a
856 shorter acquisition distance (and a greater number of photos), and the latter could
857 be avoided if a nadir-looking observation were available. In the future, the viability
858 of a nadir-looking TLS setting and a better experimental setup of SfM
859 photogrammetry should be further explored. Altogether, both TLS and SfM
860 photogrammetry provide very powerful 3D information that enables a detailed
861 analysis of surface roughness directionality, which is relevant for applications
862 such as radar scattering or hydrology and soil erosion processes.
863
864
865 **Acknowledgment**

This work was supported in part by the Spanish Ministry of Economy and Competitiveness under Grant BES-2012-054521, Project CGL2011-24336, Project CGL2015-64284-C2-1-R, and Project CGL2016-75217-R (MINECO/FEDER, EU).

References

Agisoft. 2018. Agisoft PhotoScan User Manual: Professional Edition, Version 1.4. http://www.agisoft.com/pdf/photoscan-pro_1_4_en.pdf [June, 2018].

Aguilar MA, Aguilar FJ, Negreiros J. 2009. Off-the-shelf laser scanning and close-range digital photogrammetry for measuring agricultural soils microrelief. Biosystems Engineering 103(4): 504-517. DOI: 10.1016/ j.biosystemseng.2009.02.010.

Allmaras RR, Burwell RE, Larson WE, Holt RF. 1966. Total porosity and random roughness of the interrow zone as influenced by tillage. USDA Conservation Research Report 7: 1-14.

Álvarez-Mozos J, Casalí J, González-Audícana M, Verhoest NEC. 2005. Correlation between ground measured soil moisture and RADARSAT-1 derived backscattering coefficient over an agricultural catchment of Navarre (North of Spain). Biosystems Engineering 92(1): 119-133. DOI: 10.1016/ j.biosystemseng.2005.06.008.

Álvarez-Mozos J, Verhoest NEC, Larrañaga A, Casalí J, González-Audícana M. 2009. Influence of surface roughness spatial variability and temporal dynamics on the retrieval of soil moisture from SAR observations. Sensors 9(1): 463-489. DOI: 10.3390/s90100463.

Baghdadi N, Zribi M, Loumagne C, Ansart P, Anguela TP. 2008. Analysis of TerraSAR-X data and their sensitivity to soil surface parameters over bare agricultural fields. Remote Sensing of Environment 112(12): 4370-4379. DOI: 10.1016/j.rse.2008.08.004.

Barber ME, Grings FM, Álvarez-Mozos J, Piscitelli M, Perna PA, Karszenbaum H. 2016. Effects of spatial sampling interval on roughness parameters and microwave backscatter over agricultural soil surfaces. Remote Sensing 8(6): 458. DOI: 10.3390/rs8060458.

Barneveld RJ, Seeger M, Maalen-Johansen I. 2013. Assessment of terrestrial laser scanning technology for obtaining high-resolution DEMs of soils. Earth Surface Processes and Landforms 38(1): 90-94. DOI: 10.1002/esp.3344.

Bauer T, Strauss P, Grims M, Kamptner E, Mansberger R, Spiegel H. 2015. Long-term agricultural management effects on surface roughness and consolidation of soils. Soil and Tillage Research 151: 28-38. DOI: 10.1016/j.still.2015.01.017.

Blaes X, Defourny P. 2008. Characterizing bidimensional roughness of agricultural soils surfaces for SAR modeling. IEEE Transactions on Geoscience and Remote Sensing 46(12): 4050-4061. DOI: 10.1109/TGRS.2008.2002769.

Bretar F, Arab-Sedze M, Champion J, Pierrot-Deseilligny M, Heggy E, Jacquemoud S. 2013. An advanced photogrammetric method to measure surface roughness: Application to volcanic terrains in the Piton de la Fournaise, Reunion Island. Remote Sensing of Environment 135: 1-11. DOI: 10.1016/ j.rse.2013.03.026.

Callens M, Verhoest NEC, Davidson MWJ. 2006. Parameterization of tillage-induced single-scale soil roughness from 4-m profiles. IEEE Transactions on Geoscience and Remote Sensing 44 (4): 878-888. DOI: 10.1109/TGRS.2005.860488.

Castillo RP, James MR, Quinton JN, Taguas EV, Gómez JA. 2012. Comparing the accuracy of several field methods for measuring gully erosion. Soil Science Society of America Journal 76(4): 1319-1332. DOI: 10.2136/sssaj2011.0390.

Darboux F, Huang C. 2003. An instantaneous-profile laser scanner to measure soil surface microtopography. Soil Science Society of America Journal 67: 92-99. DOI: 10.2136/sssaj2003.9200.

Davidson MWJ, Le Toan T, Mattia F, Satalino G, Manninen T, Borgeaud M. 2000. On the characterization of agricultural soil roughness for radar remote sensing studies. IEEE Transactions on Geoscience and Remote Sensing 38 (2): 630-640. DOI: 10.1109/36.841993.

Davidson MWJ, Mattia F, Satalino G, Verhoest NEC, Le Toan T, Borgeaud M, Louis JMB, Attema E. 2003. Joint statistical properties of RMS height and correlation length derived from multisite 1-m roughness measurements. IEEE

Transactions on Geoscience and Remote Sensing 41 (7): 1651-1658. DOI: 10.1109/TGRS.2003.813361.

El Hajj M, Baghdadi N, Zribi M. 2019. Comparative analysis of the accuracy of surface soil moisture estimation from the C- and L-bands. International Journal of Applied Earth Observation and Geoinformation 82: 101888. DOI: 10.1016/j.jag.2019.05.021.

FARO. 2018. User Manual for the Focus3D 20/120 and S 20/120. https://knowledge.faro.com/Hardware/Laser_Scanner/Focus/User_Manual_for_the_Focus3D_20-120_and_S_20-120 [June, 2018].

Favalli M, Fornaciai A, Isola I, Tarquini S, Nannipieri L. 2012. Multiview 3D reconstruction in geosciences. Computers & Geosciences 44: 168-176. DOI: 10.1016/j.cageo.2011.09.012.

Gilliot JM, Vaudour E, Michelin J. 2017. Soil surface roughness measurement: A new fully automatic photogrammetric approach applied to agricultural bare fields. Computers and Electronics in Agriculture 134: 63-78. DOI: 10.1016/j.compag.2017.01.010.

Glira P, Pfeifer N, Briese C, Ressl C. 2015. A correspondence framework for ALS strip adjustments based on variants of the ICP algorithm. Photogrammetrie - Fernerkundung - Geoinformation 2015(4): 275-289. DOI: 10.1127/pfg/2015/0270.

Gomez C, Hayakawa Y, Obanawa H. 2015. A study of Japanese landscapes using structure from motion derived DSMs and DEMs based on historical aerial photographs: New opportunities for vegetation monitoring and diachronic geomorphology. Geomorphology 242: 11-20. DOI: 10.1016/j.geomorph.2015.02.021.

Govers G, Takken I, Helming K. 2000. Soil roughness and overland flow. Agronomie. 20(2): 131-146. DOI: 10.1051/agro:2000114.

Helming K, Roth CH, Wolf R, Diestel H. 1993. Characterization of rainfall - microrelief interactions with runoff using parameters derived from digital elevation models (DEMs). Soil Technology 6(3): 273-286. DOI: 10.1016/0933-3630(93)90016-8.

Helming K, Römkens MJM, Prasad SN. 1998. Surface roughness related processes of runoff and soil loss: A flume study. Soil Science Society of America Journal 62(1): 243-250. DOI: 10.2136/sssaj1998.03615995006200010031x.

967 Heng BCP, Chandler JH, Armstrong A. 2010. Applying close range digital
968 photogrammetry in soil erosion studies. The Photogrammetric Record 25(131):
969 240-265. DOI: 10.1111/j.1477-9730.2010.00584.x.

970 Huang C, Bradford JM. 1992. Applications of a laser scanner to quantify soil
971 microtopography. Soil Science Society of America Journal 56(1): 14-21. DOI:
972 10.2136/sssaj1992.03615995005600010002x.

973 James MR, Robson S. 2012. Straightforward reconstruction of 3D surfaces and
974 topography with a camera: Accuracy and geoscience application. Journal of
975 Geophysical Research: Earth Surface 117(F3). DOI: 10.1029/2011JF002289.

976 James MR, Chandler JH, Eltner A, Fraser C, Miller PE, Mills JP, Noble T, Robson
977 S, Lane SN. 2019. Guidelines on the use of structure-from-motion
978 photogrammetry in geomorphic research. Earth Surface Processes and
979 Landforms (2019). DOI: 10.1002/esp.4637.

980 Jester W, Klik A. 2005. Soil surface roughness measurement—methods,
981 applicability, and surface representation. Catena. 64(2-3): 174-192. DOI:
982 10.1016/j.catena.2005.08.005.

983 Kamphorst EC, Jetten V, Guérif J, Pitkänen J, Iversen BV, Douglas JT, Paz A.
984 2000. Predicting depressional storage from soil surface roughness. Soil Science
985 Society of America Journal 64(5), 1749-1758. DOI: 10.2136/
986 sssaj2000.6451749x.

987 Magunda MK, Larson WE, Linden DR, Nater EA. 1997. Changes in microrelief
988 and their effects on infiltration and erosion during simulated rainfall. Soil
989 Technology 10(1): 57-67. DOI: 10.1016/0933-3630(95)00039-9.

990 Martinez-Agirre A, Álvarez-Mozos J, Giménez R. 2016. Evaluation of surface
991 roughness parameters in agricultural soils with different tillage conditions using a
992 laser profile meter. Soil and Tillage Research 161: 19-30. DOI: 10.1016/
993 j.still.2016.02.013.

994 Martinez-Agirre A, Álvarez-Mozos J, Lievens H, Verhoest NEC. 2017. Influence
995 of Surface Roughness Measurement Scale on Radar Backscattering in Different
996 Agricultural Soils. IEEE Transactions on Geoscience and Remote Sensing
997 55(10): 5925-5936. DOI: 10.1109/TGRS.2017.2717043.

998 Marzahn P, Rieke-Zapp D, Ludwig R. 2012a. Assessment of soil surface
999 roughness statistics for microwave remote sensing applications using a simple
1000 photogrammetric acquisition system. ISPRS Journal of Photogrammetry and
1001 Remote Sensing 72: 80-89. DOI: 10.1016/j.isprsjprs.2012.06.005.

1002 Marzahn P, Seidel M, Ludwig R. 2012b. Decomposing Dual Scale Soil Surface
1003 Roughness for Microwave Remote Sensing Applications. Remote Sensing 4(7):
1004 2016-2032. DOI: 10.3390/rs4072016.

1005 Mattia F, Davidson MWJ, Le Toan T, D'Haese CMF, Verhoest NEC, Gatti AM,
1006 Borgeaud M. 2003. A comparison between soil roughness statistics used in
1007 surface scattering models derived from mechanical and laser profilers. IEEE
1008 Transactions on Geoscience and Remote Sensing 41(7): 1659-1671. DOI:
1009 10.1109/TGRS.2003.813359.

1010 Milenković M, Pfeifer N, Glira P. 2015. Applying terrestrial laser scanning for soil
1011 surface roughness assessment. Remote Sensing 7(2): 2007-2045. DOI:
1012 10.3390/rs70202007.

1013 Mirzaei M, Ruy MS, Ziarati T, Salehi A. 2012. Monitoring of soil roughness caused
1014 by rainfall using stereo-photogrammetry. International Research Journal of
1015 Applied and Basic Sciences 3(2): 322-338.

1016 Montgomery DC. 1991. Design and analysis of experiments. John Wiley & Sons:
1017 New York, USA.

1018 Mosbrucker AR, Major JJ, Spicer KR, Pitlick J. 2017. Camera system
1019 considerations for geomorphic applications of SfM photogrammetry. Earth
1020 Surface Processes and Landforms 42(6): 969-986. DOI: 10.1002/esp.4066.

1021 Nouwakpo SK, Weltz MA, McGwire K. 2016. Assessing the performance of
1022 structure-from-motion photogrammetry and terrestrial LiDAR for reconstructing
1023 soil surface microtopography of naturally vegetated plots. Earth Surface
1024 Processes and Landforms 41(3): 308-322. DOI: 10.1002/esp.3787.

1025 Oh Y, Sarabandi K, Ulaby FT. 1992. An empirical model and an inversion
1026 technique for radar scattering from bare soil surfaces. IEEE Transactions on
1027 Geoscience and Remote Sensing 30 (2): 370-381. DOI: 10.1109/36.134086.

1028 Otepka J, Ghuffar S, Waldhauser C, Hochreiter R, Pfeifer N. 2013.
1029 Georeferenced point clouds: A survey of features and point cloud management.
1030 ISPRS International Journal of Geo-Information 2(4), 1038-1065. DOI:
1031 10.3390/ijgi2041038.

1032 Perez-Gutierrez C, Martinez-Fernandez J, Sanchez N, Alvarez-Mozos J. 2007.
1033 Modeling of soil roughness using terrestrial laser scanner for soil moisture
1034 retrieval. 2007 IEEE International Geoscience and Remote Sensing Symposium:
1035 Barcelona; 1877-1880. DOI: 10.1109/IGARSS.2007.4423190.

1036 Pfeifer N, Mandlburger G, Otepka J, Karel W. 2014. OPALS - A framework for
1037 Airborne Laser Scanning data analysis. Computers, Environment and Urban
1038 Systems 45: 125-136. DOI: 10.1016/j.compenvurbsys.2013.11.002.

1039 Rodríguez-Caballero E, Afana A, Chamizo S, Solé-Benet A, Canton Y. 2016. A
1040 new adaptive method to filter terrestrial laser scanner point clouds using
1041 morphological filters and spectral information to conserve surface micro-
1042 topography. ISPRS Journal of Photogrammetry and Remote Sensing 117: 141-
1043 148. DOI: 10.1016/j.isprsjprs.2016.04.004.

1044 Romkens MJM, Wang JY, 1986. Effect of tillage on surface roughness.
1045 Transactions of the ASAE 29(2): 429-433. DOI: 10.13031/2013.30167.

1046 Saleh A. 1993. Soil roughness measurement: chain method. Journal of Soil and
1047 Water Conservation 48(6), 527-529.

1048 SICK. 1996. Operating Instructions Distance Measuring Device.
1049 https://www.sick.com/media/docs/9/39/239/Operating_instructions_Distance_M
1050 easuring_Devise_de_en_IM0067239.PDF [September, 2019].

1051 Smith MW. 2014. Roughness in the Earth Sciences. Earth-Science Reviews 136:
1052 202-225. DOI: 10.1016/j.earscirev.2014.05.016.

1053 Snapir B, Hobbs S, Waine TW. 2014. Roughness measurements over an
1054 agricultural soil surface with Structure from Motion. ISPRS Journal of
1055 Photogrammetry and Remote Sensing 96: 210-223. DOI: 10.1016/
1056 j.isprsjprs.2014.07.010.

1057 Taconet O, Ciarletti V. 2007. Estimating soil roughness indices on a ridge-and-
1058 furrow surface using stereo photogrammetry. Soil and Tillage Research 93(1):
1059 64-76. DOI: 10.1016/j.still.2006.03.018.

1060 Thomsen LM, Baartman JEM, Barneveld RJ, Starkloff T, Stolte J. 2015. Soil
1061 surface roughness: comparing old and new measuring methods and application
1062 in a soil erosion model. Soil 1(1): 399-410. DOI: 10.5194/soil-1-399-2015.

1063 Ulaby FT, Moore RK, Fung AK. 1982. Microwave remote sensing: active and
1064 passive. Volume II. Radar remote sensing and surface scattering and emission
1065 theory. Addison-Wesley: Reading, MA, USA.

1066 Verhoest NEC, Lievens H, Wagner W, Álvarez-Mozos J, Moran MS, Mattia F.
1067 2008. On the soil roughness parameterization problem in soil moisture retrieval
1068 of bare surfaces from synthetic aperture radar. Sensors. 8(7): 4213-4248. DOI:
1069 10.3390/s8074213.

1070 Vermang J, Norton LD, Baetens JM, Huang C, Cornelis WM, Gabriels D. 2013.
1071 Quantification of soil surface roughness evolution under simulated rainfall.
1072 Transactions of the ASABE 56(2): 505-514. DOI: 10.13031/2013.42670.

1073 Vidal Vázquez E, Vivas Miranda JG, Paz González A. 2005. Characterizing
1074 anisotropy and heterogeneity of soil surface microtopography using fractal
1075 models. Ecological Modelling 182(3-4): 337-353. DOI: 10.1016/
1076 j.ecolmodel.2004.04.012.

1077 Wegmüller U, Santoro M, Mattia F, Balenzano A, Satalino G, Marzahn P, Fischer
1078 G, Ludwig R, Floury N. 2011. Progress in the understanding of narrow directional
1079 microwave scattering of agricultural fields. Remote Sensing of Environment
1080 115(10): 2423-2433. DOI: 10.1016/j.rse.2011.04.026.

1081 Woodget AS, Carbonneau PE, Visser F, Maddock IP. 2015. Quantifying
1082 submerged fluvial topography using hyperspatial resolution UAS imagery and
1083 structure from motion photogrammetry. Earth Surface Processes and Landforms
1084 40 (1): 47-64. DOI: 10.1002/esp.3613.

1085 Xingming Z, Kai Z, Xiaojie L, Yangyung L, Jianhua R. 2014. Improvements in
1086 farmland surface roughness measurement by employing a new laser scanner.
1087 Soil and Tillage Research 143: 137-144. DOI: 10.1016/j.still.2014.06.010.

1088 Zribi M, Muddu S, Bousbih S, Al Bitar A, Tomer SK, Baghdadi N, Bandyopadhyay
1089 S. 2019. Analysis of L-Band data for soil moisture estimations over agricultural
1090 areas in the tropics. Remote Sensing 11(9): 1122. DOI: 10.3390/rs11091122.

1091